Macromolecular Research

Volume 17, Number 6 June 25, 2009

Feature Article

New Characterization Methods for Block Copolymers and their Phase Behaviors

Hae-Woong Park, Jueun Jung, and Taihyun Chang*

Department of Chemistry and Graduate Institute of Advanced Materials Science, Pohang University of Science and Technology, Pohang 790-784, Korea

Received May 11, 2009; Revised June 8, 2009; Accepted June 9, 2009

Abstract: In this feature article, we briefly review the new methods we have utilized recently in the investigation of morphology and phase behavior of block copolymers. We first describe the chromatographic fractionation method to purify block copolymers from their side products of mainly homopolymers or block copolymer precursors inadvertently terminated upon addition of the next monomer in the sequential anionic polymerization. The chromatographic method is extended to the fractionation of the individual block of diblock copolymers which can yield the diblock copolymer fractions of different composition and molecular weight, which also have narrower distributions in both molecular weight and composition. A more detailed phase diagram could be constructed from the set of block copolymer fractions without the need of acquiring many block copolymers each prepared by anionic polymerization. The fractions with narrow distribution in both molecular weight and composition exhibit better long-range ordering and sharper phase transition. Next, epitaxial relationships between two ordered structures in block copolymer thin film is discussed. We employed the direct visualization method, transmission electron microtomography (TEMT) to scrutinize the grain boundary structure.

Keywords: block copolymer, molecular characterization, chromatography, phase transition, epitaxial grain boundary, transmission electron microtomography.

Introduction

Nano-structured materials have been drawing much attention in recent years due to their high potential in applications to various emerging nanotechnology. Among the nano-structured materials, block copolymer is one of the most intensively studied materials for the past decades.[1-29] Block copolymers are composed of two or more chemically different polymers, which are covalently linked each other. They self-assemble spontaneously to form various ordered nano-structures with several tens of nm length scale. For diblock copolymers, which consist of two different polymers, the segregation of the block components due to thermodynamic incompatibility and the connectivity of the two chains yields various nano-structures such as lamellar (LAM), hexagonally packed cylinder (HEX), spheres arranged in body centered cubic lattice (BCC), double gyroid (DG) and hexagonally perforated lamellar (HPL) in bulk as well as in solution.[2,24,30-36] Figure 1(a) shows an overview of the most commonly observed morphologies of diblock copolymers.[37] The morphology of the microphase-separated domains is governed by the degree of polymerization, the volume fraction of

*Corresponding Author. E-mail: tc@postech.ac.kr

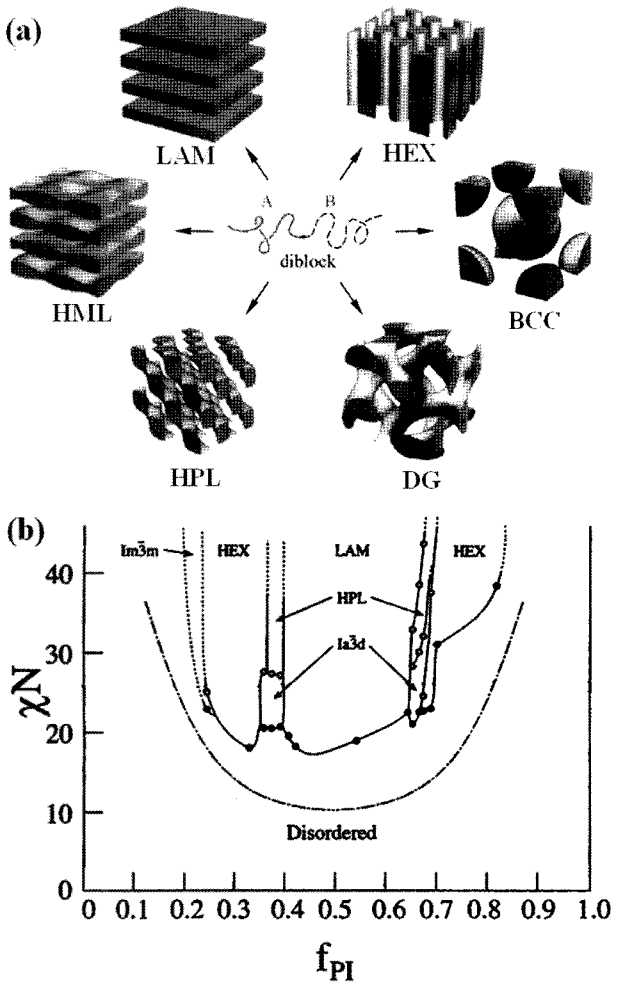

Figure 1. (a) Most commonly observed morphologies in diblock copolymers. LAM: lamellar, HEX: hexagonally packed cylinder, BCC: spheres arranged in BCC lattice, DG: double gyroid, HPL: hexagonally perforated lamellar, HML: hexagonally modulated lamellar. Reproduced with permission from Ref. 37; Copyright 1998, WILEY-VCH Verlag GmbH & Co. KGaA. (b) Experimentally constructed phase diagram of polystyrene-*block*-polyisoprene (PS-*b*-PI). Reproduced with permission from Ref. 38; Copyright 1995, ACS publications.

each block, and the Flory-Huggins interaction parameter, χ, as shown in an experimentally constructed phase diagram (Figure 1(b)).[38]

Depending on the degree of incompatibility χN, several regimes have been identified along the composition axis of the copolymer, the volume fraction of one component, f for a diblock copolymer. For a symmetric diblock copolymer of $f = 0.5$, χN value at the order-disorder transition (ODT), $(\chi N)_{ODT} = 10.5$ in the mean field limit.[39] The weak segregation limit (WSL) corresponds to χN close to $(\chi N)_{ODT}$ extending to $\chi N \approx 12$, as estimated by Matsen and Bates.[40] The intermediate segregation regime ranges up to about $\chi N \approx 100$, and the strong segregation limit (SSL) extends to higher incompatibilities. Between WSL and SSL lies a regime exhibiting a complicated phase behavior which reflects a delicate balance between entropic and energetic contributions to the overall free energy. At the time of first discovery of the microphase of block copolymers, it was thought that phase-separated morphology is fixed at a given block volume fraction. However, order-order transition (OOT) phenomena depending on temperature have been reported in various diblock copolymers and it was shown theoretically that the OOT of phase-separated microdomains can occur in the WSL regime upon changing temperature.[39]

During the past decades the structure and properties of diblock copolymers have been investigated near WSL. Many model block copolymers have been prepared and characterized by rheological methods, small-angle neutron and X-ray scattering (SANS and SAXS) and transmission electron microscopy (TEM).[2,30,38,41,42] At least the existence of six distinct microstructures was confirmed as shown in Figure 1(a). Three of these have been documented in the early stage of experimental studies of block copolymers: spheres arranged in a BCC lattice ($Im\bar{3}m$ space group), HEX and LAM. The other three microstructures have also been identified later, located between the HEX and LAM phases. Modulated (ML) and perforated (PL) lamellar structures stacked with hexagonal symmetry, denoted as HML and HPL, respectively, have been documented in a variety of block copolymers.[43,44] Double gyroid (DG), bicontinuous cubic phase with $Ia\bar{3}d$ space group symmetry, has also been found.[45] The OOT often exhibits epitaxial relationship between the geometries of the two phases.[12,13,29,38,44,46-67] For example, the transition from hexagonally packed cylinder phase to the body centered cubic (BCC) phase occurs through initial undulation of the cylinders before they divide into spheres, which eventually converts the cylinder axis to the [111] direction of BCC structure.[46,50,57-60,68]

For synthesis of block copolymers, a number of different polymerization methods have been utilized.[69-75] Among them, anionic polymerization is the best method to yield the polymers with narrow molecular weight distribution (MWD).[69,70] By virtue of little side reactions in the anionic polymerization, molecular weight and composition of synthesized block copolymer can be easily predicted from the ratio of initiator and each monomers added. Block copolymers prepared by anionic polymerization are often regarded as "monodisperse" although the MWD of each block is far from the rigorous meaning of the term. The MWD of synthetic polymers is commonly measured by size exclusion chromatography (SEC).[76-78] However, the resolution of SEC is not high enough to provide a correct MWD of polymers prepared by anionic polymerization. Interaction chromatography (IC) was found to allow a much higher resolution for the MWD analysis of polymers.[79-84] An IC analysis on MWD of a set of polystyrenes prepared from a single batch anionic polymerization showed that the true MWD is much narrower than that mea-

sured by SEC.[79,85] Their MWD was found quite close to the Poisson distribution as predicted by Flory a long time ago.[86] Nonetheless, it still has a finite MWD. Consequently each block of a block copolymer has a finite MWD, which leads to chemical composition distribution (CCD) in a whole ensemble of block copolymer molecules. It is of interest to find out a rigorous MWD and CCD of block copolymers and how the distributions affect the phase behavior of block copolymers.

In this feature article, we briefly review the new methods we have utilized recently in the investigation of block copolymer morphology and its phase behavior. We first discuss on the chromatographic fractionation method to purify a block copolymer from its side products mainly the homopolymer or block copolymer precursors inadvertently terminated upon addition of the next monomer in the sequential anionic polymerization. The chromatographic method was extended to the fractionation of the individual block of diblock copolymers which results the fractionation of a diblock copolymer according to both molecular weight and composition. We were able to construct a detailed phase diagram from the set of block copolymer fractions without synthesizing many individual block copolymers. The fractions have narrow distribution in both molecular weight and composition and exhibit improved long range ordering and sharper phase transition. Next, epitaxial relationships between two ordered structures in block copolymer thin film will be discussed. As we already mentioned, epitaxial relationship in the order-order transition of block copolymers have been extensively studied. Most of the studies utilized SAXS or SANS. Such scattering methods provide averaged information on the structure and the orientation of the domain structure is required to extract the useful information on the epitaxial relationship in the order-order transition. Nonetheless, detailed structural information at the grain boundary is not accessible from the scattering measurements. We employed the direct visualization method, transmission electron microtomography (TEMT) to scrutinize the grain boundary structure.[29,67,87-89]

Chromatographic Purification of Block Copolymers from Precursors.[9-11,90] We chose a polystyrene-*block*-polyisoprene (PS-*b*-PI) diblock copolymer to demonstrate the unique capability of chromatographic purification of block copolymers from the homo-PS precursor contamination. The chromatographic purification scheme is illustrated in Figure 2(a).[10] It is essentially the same method to separate two different polymers by simultaneous SEC and IC.[91,92] In this application, the two different polymers are homo-polymer precursor and block copolymer. The chromatographic separation condition is established in such a way to elute PS without interaction with the column stationary phase. For the purpose, a C18 bonded silica HPLC column with CH_2Cl_2/CH_3CN =74/26 (v/v) as a mobile phase is employed. In this separation condition, the PS precursor elutes before the injection

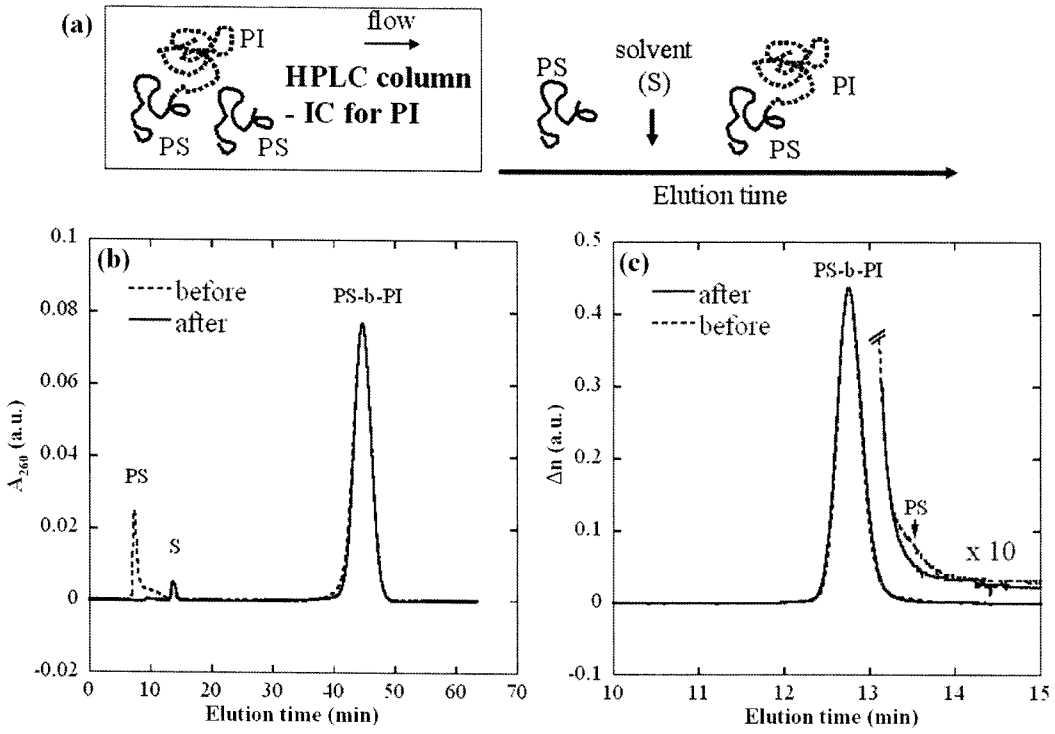

Figure 2. (a) The scheme of chromatographic purification. Homo PS precusor is eluted earlier than PS-*b*-PI because PI interacts with stationary phase. (b) TGIC and (c) SEC profiles of PS-*b*-PI diblock copolymers before and after the homopolymer PS removal. A fraction of the SEC signals was increased ten-fold ("x 10") in (c) to highlight the SEC profile change before and after the PS removal. Reproduced with permission from Ref. 10; Copyright 2004, ACS publications.

solvent peak in the SEC separation mode while PS-*b*-PI elutes after the solvent peak due to the stronger interaction of the PI block with the stationary phase (IC separation mode). Figure 2(b) and (c) contrast the IC and SEC profiles before and after the PS homopolymer removal for the as-synthesized PS-*b*-PI (32 k-31 k), which contains 6 wt% PS predursor (32 k). Distinctive chromatographic separation of the homo-PS from the PS-*b*-PI was possible, because the PI-adsorbing IC conditions caused the elution of PS before the solvent peak, whereas PS-*b*-PI elution occurred after the solvent peak (Figure 2(b)). It is like a "filtering" technique relying on the retention time difference for the HPLC separation. Another advantage of the IC technique is that it enables *semi-prep scale separation* of block copolymers through multiple injections.[10,11,90]

In contrast, SEC analysis in THF before and after PS removal gave the same M_w/M_n value of 1.02 and the homopolymer removal effect only appeared as a slight change in the lower molecular weight tails of the SEC profile (Figure 2(c)). Thus, SEC is a poor choice for block copolymer analysis, since it separates polymer chains only according to their hydrodynamic size.

Fractionation of Individual Blocks by Two Dimensional Chromatography (2D-LC).[9-11,17,93] The precise characterization of a copolymer is much more complicated than that of a homopolymer since copolymers have bivariate distribution in both molecular weight and composition. The ultimate goal is to construct a two-dimensional, one in molecular weight and the other in chemical composition, distribution map. An attractive method for this purpose is two-dimensional liquid chromatography (2D-LC), in which two different chromatographic separation methods are used in sequence.[94-97] If one of the two separation methods is sensitive to one molecular characteristic while not to the other, and vice versa, it would be possible to construct such a 2D distribution map. For the fractionation of a block copolymer, we employed 2D-LC method; normal phase liquid chromatography (NPLC) for one dimension and reversed phase liquid chromatography (RPLC) dimension for the other dimension. The strategy is to separate one block in terms of its molecular weight with minimal effect of the other block. We applied this method for the separation of PS-*b*-PI diblock copolymer, which has been used extensively for the morphological study of block copolymers.[8,64,85,93] The contrast in polarity of PS-*b*-PI is subtle but we found that suitable IC conditions could be established for the separation of individual blocks with little effect from the presence of the other block.

Figure 3 shows a 2D-LC chromatogram of low MW PS-*b*-PI in which the molecular weight distribution of the two individual blocks is completely mapped.[17] The 2D-LC consists of normal phase liquid chromatography (NPLC) for one dimension and reversed phase liquid chromatography (RPLC) for the other dimension. The 1st-D NPLC separates PS-*b*-PI according to the PS block length while the 2nd-D RPLC separates PS-*b*-PI according to the PI block length. For the 1st-D NPLC separation, the column temperature was controlled to improve the resolution[83,84] while the 2nd-D RPLC was run isothermally to reduce the separation time. The molecular weight distribution information of individual blocks provides with equivalent information to molecular weight distribution and chemical composition distribution of a block copolymer. In this analysis, the effluent from the 1st-D LC separation is concentrated before the injection to the 2nd-D LC by use of a trap-column, which allows an efficient interface between the two LC separations. Over 200 different block copolymer species could be identified from the 2D-LC chromatogram.

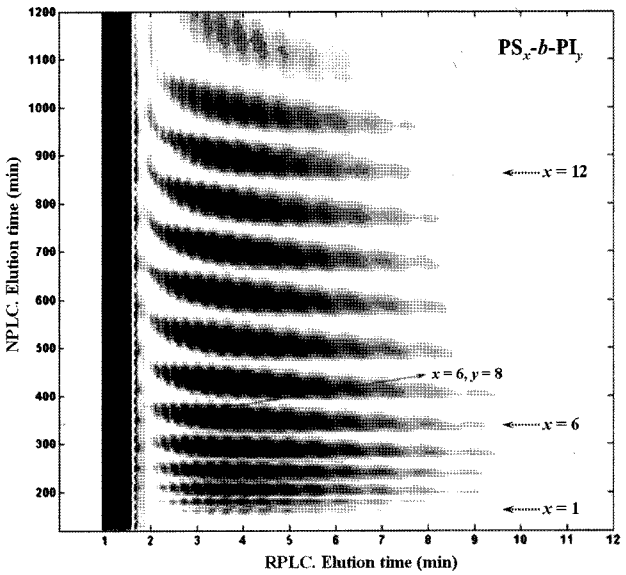

Figure 3. NPLC×RPLC 2D-LC chromatogram of low MW PS-*b*-PI. The 1st-D NPLC separates PS-*b*-PI according to the PS block length while the 2nd-D RPLC separates PS-*b*-PI according to the PI block length. For the 1st-D NPLC separation, the column temperature was controlled to improve the resolution while the 2nd-D RPLC was run isothermally to reduce the separation time. Reproduced with permission from Ref. 17; Copyright 2007, ACS publications.

Phase Diagram Constructed by 2D-LC Fractions.[93,64] In order to construct a phase diagram of block copolymer species, an enough number of samples with different compositions and with appropriate molecular weight (having proper χN value) are needed. However, it is nontrivial to acquire a desirable set of block copolymers. If appropriate samples are not available, the samples of different compositions are mixed sometimes to prepare the wanted composition of block copolymer, but it inevitably increases the MWD of the block copolymers. Herein, we used an opposite strategy to adjust the composition; instead of mixing block copolymers of different composition, we fractionated an anionic-polymerized diblock copolymer to obtain a set of block copolymers with different composition. In this way, we can

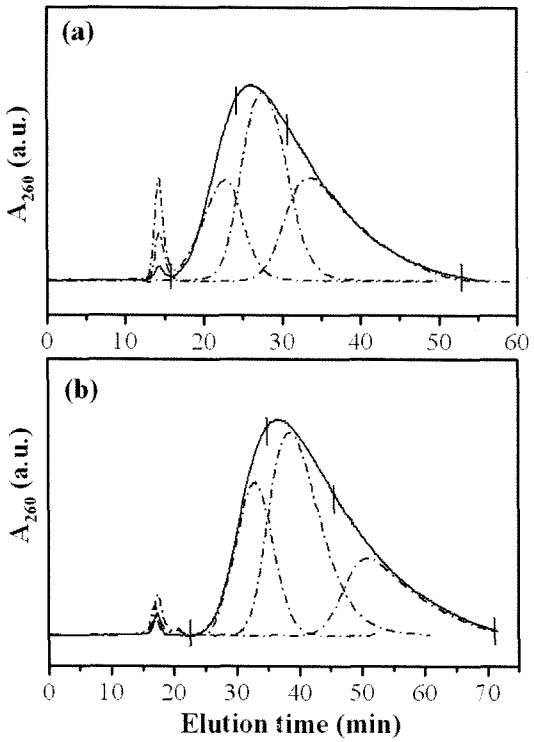

Figure 4. 2D-LC fractionation of PS-*b*-PI (24 k, 34.8 wt% PI content). (a) RPLC chromatograms of the mother PS-*b*-PI (solid line) and its three fractions (dash-dot line). (b) NPLC chromatograms of the middle fraction of RPLC separation (solid line) and its three fractions (dash-dot line). RPLC fractionates the PI block while NPLC fractionates the PS block. The range of the fraction collected is indicated with small vertical bars. Reproduced with permission from Ref. 93; Copyright 2002, ACS publications.

work with a set of block copolymers of wanted composition and with narrower distribution in both molecular weight and composition.

We applied 2D-LC method for the separation of PS-*b*-PI diblock copolymer, which has been used extensively for the morphological study of block copolymers.[8,64,85,93] Figure 4 shows RPLC and NPLC chromatograms of PS-*b*-PI (24 k, 34.8 wt% PI content). In order to fractionate PI block, we used RPLC system operated at 15 °C with C18 bonded silica and a mixture of CH_2Cl_2/CH_3CN (75/25, v/v) as stationary and mobile phase, respectively. And for NPLC system in which PS-*b*-PI can be fractionated in terms of PS block length, a diol bonded silica and isooctane/THF (70/30, v/v) were used as stationary and mobile phase, respectively, at 32 °C. The mother block copolymer was fractionated into nine fractions, three fractions each by NPLC and RPLC. Figure 4(a) displays the RPLC chromatograms of the mother copolymer (solid line) and its low, middle and high molecular weight fractions in PI block (dash-dot line) separated by RPLC. Figure 4(b) shows the NPLC chromatograms of the RPLC middle fraction in Figure 4(a) (solid line) and its three

Table I. Characteristics of the PS-*b*-PI Block Copolymers Showing Variations in Composition as well as in Molecular Weight. Reproduced with Permission from Ref. 93; Copyright 2002, ACS Publications

Mother PS-*b*-PI (M_n=23.4 k, 34.8 wt% PI content)				
Sample Code[a]		NPLC		
		S_L	S_M	S_H
RPLC	I_H	21.8 k[b] 39.0 wt%[c]	23.5 k 37.6 wt%	25.2 k 35.3 wt%
	I_M	21.4 k 37.2 wt%	23.0 k 34.8 wt%	24.5 k 31.9 wt%
	I_L	21.0 k 32.3 wt%	22.5 k 32.1 wt%	24.0 k 30.4 wt%

[a]*S* and *I* stand for PS and PI block fractionated by NPLC and RPLC, respectively. Subscripts, *L*, *M* and *H* stand for low, medium and high molecular weight fractions, respectively. [b]Number average molecular weights determined by SEC. [c]Weight fraction of PI block determined by ^{1}H NMR spectroscopy.

fractions (dash-dot line) that have different PS content. Small vertical bars on the solid line chromatogram indicate the portions collected. In this way, nine fractions of the mother PS-*b*-PI with different molecular weights and weight fractions were obtained. The fractionated PS-*b*-PIs were characterized by SEC-light scattering detection for the average molecular weight and ^{1}H NMR for the composition and the results are summarized in Table I.

As we mentioned above, the cross fractionation by RPLC and NPLC yields the block copolymers with a narrower distribution in molecular weight as well as in chemical composition, which exhibit significant variations in average molecular weight (ca. 15% difference) as well as in composition (ca. 10% difference). These variations were large enough to show different morphologies and phase transition temperatures for the fractions from a single mother block copolymer. Therefore we selected PS-*b*-PI (M_n=34.0 k, 63.4 wt% PI content, M_w/M_n=1.02), which have a composition between LAM and HEX, and could construct the detailed phase diagram of PS-*b*-PI over a composition range about 10%. The molecular weights, compositions of the fractionated PS-*b*-PIs were listed in Table II.

Figure 5 displays the SAXS profiles measured at room temperature of the mother PS-*b*-PI and its nine fractions prepared by 2-D LC fractionation as shown above. The samples were annealed at 120 °C. The morphologies of the samples was also confirmed by TEM since the morphology of block copolymer, such as HPL structure,[98] is sometimes difficult to be determined by SAXS profile only. A TEM micrographs of the mother PS-*b*-PI and its HPLC fractions are shown in Figure 6. In the TEM micrograph, the PI phase appears dark since OsO_4 preferentially stains the double bonds in the PI block. The TEM picture shows the dark PI lamellae are perforated by light PS domain.

Table II. Molecular Characteristics and Phase Behavior of the PS-*b*-PI Block Copolymers. Reproduced with Permission from Ref. 64; Copyright 2003, ACS Publications

Mother PS-*b*-PI (M_n=34.0 k, f_{PI}=0.665, HPL $\xrightarrow{170^\circ C}$ DG $\xrightarrow{230^\circ C}$ Dis)				
Sample Code[a]		NPLC		
		S_L	S_M	S_H
RPLC	I_H	33.2 k[b] 0.706[c] HEX $\xrightarrow{200^\circ C}$ Dis[d]	34.8 k 0.687 DG $\xrightarrow{170^\circ C}$ HEX $\xrightarrow{210^\circ C}$ Dis	35.0 k 0.672 DG $\xrightarrow{205^\circ C}$ HEX $\xrightarrow{230^\circ C}$ Dis
	I_M	30.8 k 0.675 DG $\xrightarrow{180^\circ C}$ HEX $\xrightarrow{210^\circ C}$ Dis	32.7 k 0.657 HPL $\xrightarrow{165^\circ C}$ DG $\xrightarrow{220^\circ C}$ Dis	34.3k 0.637 LAM $\xrightarrow{165^\circ C}$ HPL $\xrightarrow{190^\circ C}$ DG $\xrightarrow{240^\circ C}$ Dis
	I_L	30.6 k 0.638 HPL $\xrightarrow{165^\circ C}$ DG $\xrightarrow{245^\circ C}$ Dis	31.2 k 0.627 LAM $\xrightarrow{190^\circ C}$ DG $\xrightarrow{230^\circ C}$ Dis	32.4 k 0.608 LAM $\xrightarrow{245^\circ C}$ Dis

[a]*S* and *I* stand for PS and PI block fractionated by 2D-LC. Subscripts, *L*, *M* and *H* stand for low, medium and high molecular weight fractions, respectively. [b]Number average molecular weight determined by SEC-Light scattering. [c]Volume fraction of PI block determined by ^{1}H NMR spectroscopy. [d]LAM: lamellae, HPL: hexagonally perforated layers, DG: double gyroid, HEX: hexagonally packed cylinder, Dis: disordered phase.

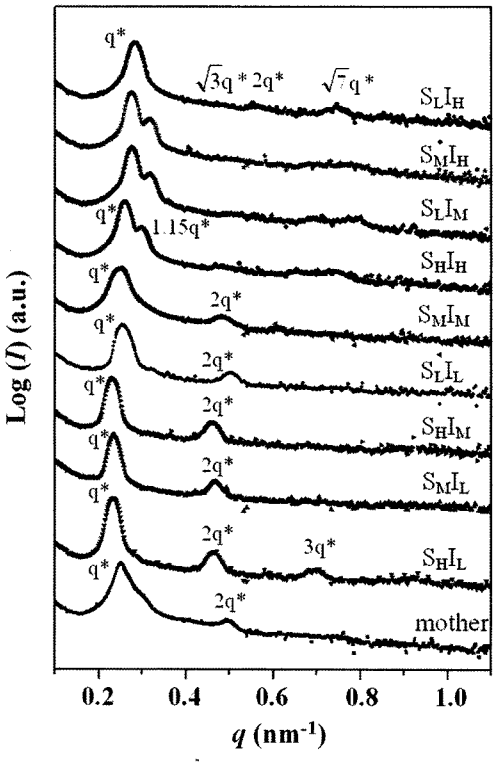

Figure 5. SAXS profiles of mother PS-*b*-PI and the fractions annealed at 120 °C. They show a variety of morphologies. Reproduced with permission from Ref. 64; Copyright 2003, ACS publications.

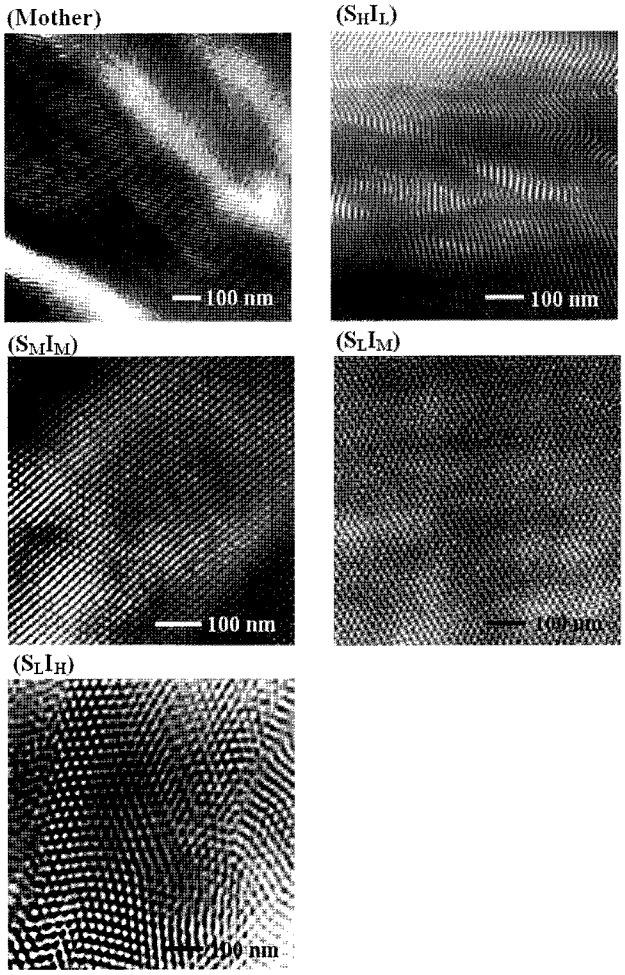

Figure 6. TEM micrographs of the mother PS-*b*-PI and its HPLC fractions. The HPLC fractions show very clear morphology, in particular a well-developed HPL microdomain structure was observed for S_MI_M that was not shear aligned. Reproduced with permission from Ref. 64; Copyright 2003, ACS publications.

Phase behaviors (OOTs and ODTs) of block copolymer systems have been studied by various techniques such as SAXS, rheology, birefringence, etc.[99-104] We used SAXS to investigate the phase behavior. The OOT temperature can be determined by a discontinuity in the plot of the reciprocal of the first-order peak maximum intensity ($1/I_m$) vs. the reciprocal of the absolute temperature ($1/T$). Also OOT sometimes accompanies an abrupt change of the domain spacing ($D=2\pi/q^*$). The ODT temperature can be obtained by a point where the maximum scattered intensity decreases sharply. In this way we could measure the OOT and ODT temperatures of the mother PS-*b*-PI and the nine fractions. The results are summarized in Table II and a detailed phase diagram of χN vs. PI volume fraction (f_{PI}) was constructed as displayed in Figure 7.

In Figure 7, the squares, circles, triangles, and stars stand for LAM, HPL, DG and HEX morphologies found in the

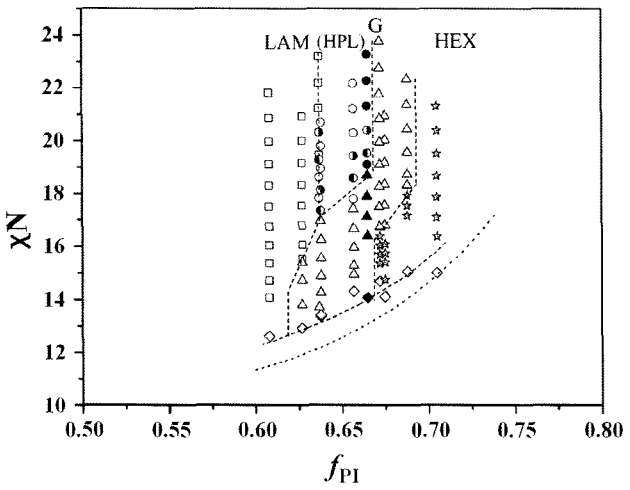

Figure 7. Phase diagram of PS-*b*-PI constructed with the fractionated PS-*b*-PIs. Different symbols stand for the different morphologies as shown in the figure. Filled symbols represent the mother PS-*b*-PI. The dotted line is the ODT calculated according to the mean filed theory while rhombuses are the measured ODT. The dashed line is the phase boundary drawn for visual aid. Half-filled circles represent the data points to test the stability of HPL phase. Refer to the text for details. Reproduced with permission from Ref. 64; Copyright 2003, ACS publications.

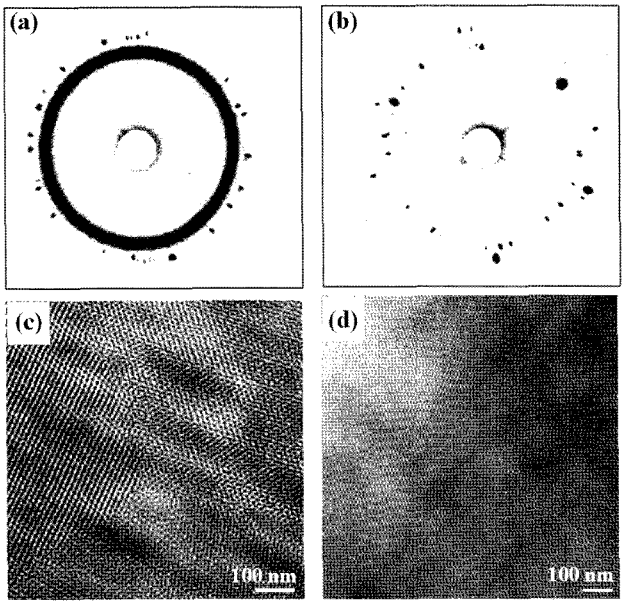

Figure 8. 2D SAXS patterns of (a) unfractionated PS-*b*-PI and (b) fractionated PS-*b*-PI, which exhibit DG morphology in bulk. TEM images of (c) unfractionated PS-*b*-PI and (d) fractionated PS-*b*-PI. A single grain DG structure over the entire image is shown in fractionated sample, while a multi-grain structure is evident in unfractionated one. Reproduced with permission from Ref. 28; Copyright 2008, Elsevier.

SAXS measurements, respectively. The rhombuses are ODT points and the filled symbols represent the mother PS-*b*-PI. The points in one vertical line (a constant f_{PI}) represent the data set for a PS-*b*-PI sample measured at different temperatures. Therefore there are ten lines for the nine fractions and the mother PS-*b*-PI, covering about 10% in the PI volume fraction. Dotted line is the mean field prediction of the ODT and the dashed line is the phase boundary drawn for visual aid. While the general feature of this phase diagram is similar to the results of Khandpur *et al.*,[38] it shows the very fine details of the phase behavior near ODT over the narrow composition range, which would not be easy to be obtained without such a well-defined set of the polymer samples of the similar molecular weights and compositions. The phase behavior of the mother PS-*b*-PI including OOT and ODT points is not much distinguishable from the fractions although the TEM image in Figure 6 shows a much clearer HPL structure for the S_MI_M fraction than the mother PS-*b*-PI. The large grain size of the S_MI_M fraction is likely due to the narrower distribution in molecular weight and composition.

Molecular Weight Distribution Effect on the Morphological Behavior of Diblock Copolymer.[28] Molecular weight distribution effect on the morphological behavior of PS-*b*-PI diblock copolymers was investigated. The PS-*b*-PI samples were prepared by anionic polymerization and further fractionated by 2D-LC to obtain the fractions of similar average molecular weight and composition but of narrower distributions in both molecular weight and composition. The interfacial thickness, grain size and the phase transition behavior of the unfractionated and fractionated PS-*b*-PI were compared by X-ray reflectivity (XR), SAXS, TEM and theological measurements. The fractionated PS-*b*-PI with more homogeneous molecular weight and composition exhibits a narrower interface, larger grain size and a sharper morphological transition compared to the unfractionated PS-*b*-PI.

Figure 8(a) and (b) display 2D SAXS profiles of the unfractionated and the fractionated PS-*b*-PI, which shows DG structure, respectively. 2D SAXS image of the unfractionated sample shows a discrete diffraction pattern from the {220} plane while a continuous ring pattern from the {211} plane. Such a speckle pattern indicative of the long-range ordering or large grain size has been reported previously by Hajduk *et al.* for a PS-*b*-PI system after transforming the lamellar phase to the gyroid phase by annealing.[45] In case of the fractionated sample, the speckle pattern becomes much more pronounced to show strong diffraction spots from both {211} and {220} planes as can be seen in Figure 8(b). Figure 8(c) and (d) show TEM images of the fractionated and unfractionated samples, respectively. A single grain double gyroid structure larger than 1×1 μm area was observed for the fractionated sample, while multi-grain structure is evident in the case of unfractionated one. These results also indicate clearly that the homogeneity of block copolymers leads to a larger grain size in the phase-segregated morphology.

Figure 9 displays XR profiles and their corresponding electron density profiles of PS-*b*-PI thin films on a Si wafer.

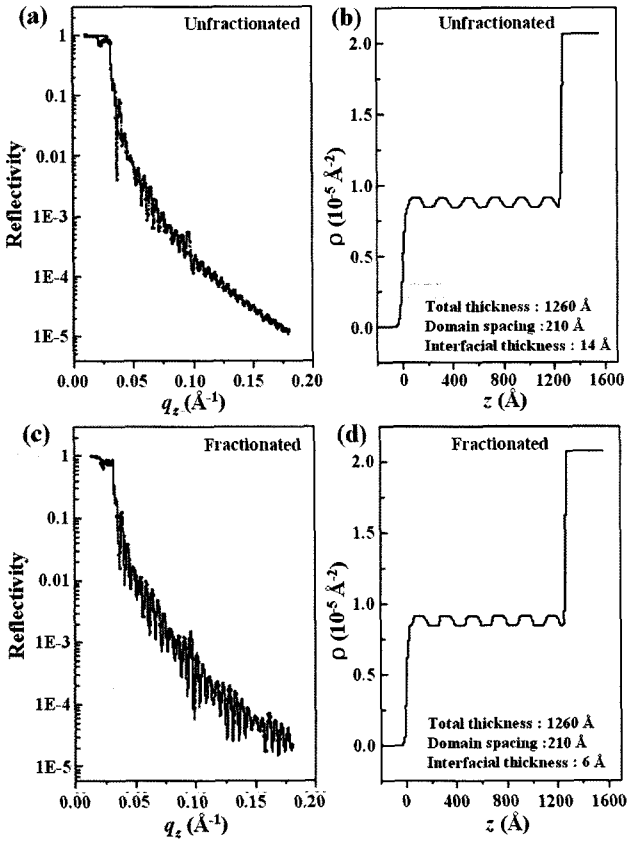

Figure 9. (a) X-ray reflectivity curve and (b) electron density profile of the unfractionated PS-*b*-PI which exhibits LAM phase in thin film. (c) X-ray reflectivity curve and (d) electron density profile of the fractionated PS-*b*-PI. The filled squares and the solid line represent the experimental data and the fitted curve, respectively. Reproduced with permission from Ref. 28; Copyright 2008, Elsevier.

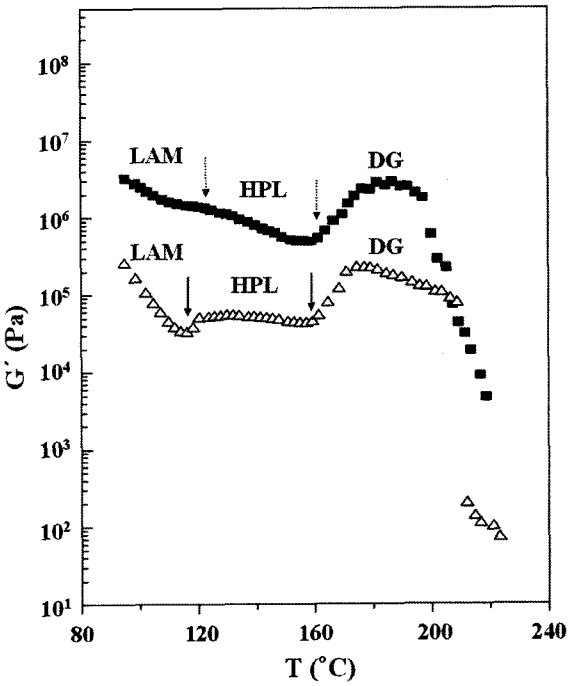

Figure 10. Dynamic storage modulus (G') as a function of temperature for the unfractionated (■) and the fractionated (△) PS-*b*-PI. Data of the unfractionated sample are vertically shifted by multiplying 100 for visual clarity. The fractionated sample exhibited morphological transitions more clearly than that of the unfractionated PS-*b*-PI. The arrows indicate the phase transition temperatures determined from the SAXS measurements. Reproduced with permission from Ref. 28; Copyright 2008, Elsevier.

These block copolymers have a symmetric composition and the lamellae of PS and PI domains are oriented parallel to the substrate plane. Once q exceeds the critical angle of the substrate, a significant portion of the X-ray beam penetrates into the substrate and a sharp drop of the reflected intensity occurs. The steeply decaying reflectivity curve is modulated by Kiessig fringes.[105] These fringes appear due to the interference between the X-ray beams reflected from the film surface and from the film/substrate interface. Also the amplitude of Kiessig fringes is modulated at a lower frequency, which arises from the layer structure of the PS and PI domains. The modulating Kiessig fringes of the fractionated PS-*b*-PI show up much more clearly than the unfractionated PS-*b*-PI indicative of the sharper contrast in internal domain structure. The film depth profile including the interfacial thickness can be estimated from the analysis of the XR curve. The XR data are fit with a nonlinear least squares algorithm using the recursive multilayer method of Parratt[106] and the fit parameters for PS, PI and Si wafer in the literature.[107] By fitting the XR profiles to the model, the internal structure of the thin films can be extracted. In Figure 9(b) an (d), the electron density profiles of PS-*b*-PI thin films are shown, from which we can note that the electron density profile in the fractionated sample shows a higher contrast than the unfractionated sample. While the total film thickness and the domain spacing are very similar at 1,260 Å and at 210 Å for the both thin films, the interfacial thickness between the two block domains shows a clear difference: 14 Å for the unfractionated PS-*b*-PI and 6 Å for fractionated PS-*b*-PI. It is clear that the homogeneity of the block copolymer leads to a better-developed internal structure of the phase-segregated morphology.

We also investigated the effect of the fractionation on the OOT and ODT of the block copolymers. The phase transition behavior of PS-*b*-PI, which exhibits HPL →DG→ disordered structures upon heating, was monitored by rheological measurements. Figure 10 shows the change of the dynamic storage modulus as a function of temperature. The phase transition temperatures determined by rheological measurements are consistent with the previous SAXS results[64] indicated with arrows. However, the fractionated sample exhibited much sharper morphological transitions than that of the

unfractionated PS-*b*-PI.

Epitaxial Relation between Two Ordered Structures in Block Copolymer Thin Film.[12,13,29,67] Many research results can be found in the literature for the epitaxial relationship, most of which are based on the small angle scattering method for the structural analysis of block copolymers. However, there is a limitation in the detailed analysis of the transitional relationship since the data acquired from the scattering measurements provide with the averaged structural information only and it is difficult to extract the detailed structure near grain boundary between two ordered phases in real space. Moreover, well-oriented structures by external force, such as shearing, are needed for the analysis of epitaxial relationship between two ordered structures.[44,49,54,55,57-59,62,63] Although TEM has been used for the visualization of structure as a complementary tool, it provides 2-dimensional structure only and it is often difficult to elucidate the detailed epitaxial relationship in the grain boundary.

Transmission electron microtomography (TEMT) is an emerging technique for the visualization of inner structure 3-dimensionally.[29,67,87-89] TEMT is a tool combining TEM and computerized tomography (CT). The CT scan is a well-established medical equipment using X-ray to produce multiple images or pictures of the human body taken at different observation angles and finally a computer joins them together to obtain cross-sectional view of the area being examined. In this case, the detector-source arrangement is tilted relative to the patient around a single axis, while the beam direction is fixed and the specimen holder is tilted around a single axis in TEMT. TEMT uses a series of 2D projections taken by TEM and it offers a new approach to obtain 3D information in nanometer scale.

In most studies concerning the epitaxial phase transition between two ordered structures, shear aligned phases were used for detailed X-ray or neutron scattering analysis.[44,49,54,55,57,62,63] Instead of aligning the grains by shearing, we used thin film since the structures in thin film are oriented along the film plane in thin films. Considering the phase transition from HPL to DG in thin film, the layers in the HPL structure are converted to $\{121\}_{DG}$ structure maintaining their orientation parallel to the film plane. The perforations in the HPL structure in PS-*b*-PI thin film was found to have the ABC type stacking without detectable defects by grazing incidence small-angle X-ray scattering (GISAXS) as shown in Figure 11(a).[12,13] The GISAXS patterns appear not ring-shaped but as discrete spots, which correspond to the diffraction patterns that the layers of HPL and planes of $\{121\}_{DG}$ are parallel to the substrate plane but randomly oriented in-plane.[12,13,108] Figure 11(c) shows a cross-sectional TEM image of the HPL structure. PI domains were selectively stained by OsO_4 and appear darker than PS domains. Because PS is a minor component of this diblock copolymer, the layers of PS block are perforated by PI blocks. The HPL layers are well aligned parallel to the substrate as expected from the GISAXS pattern.

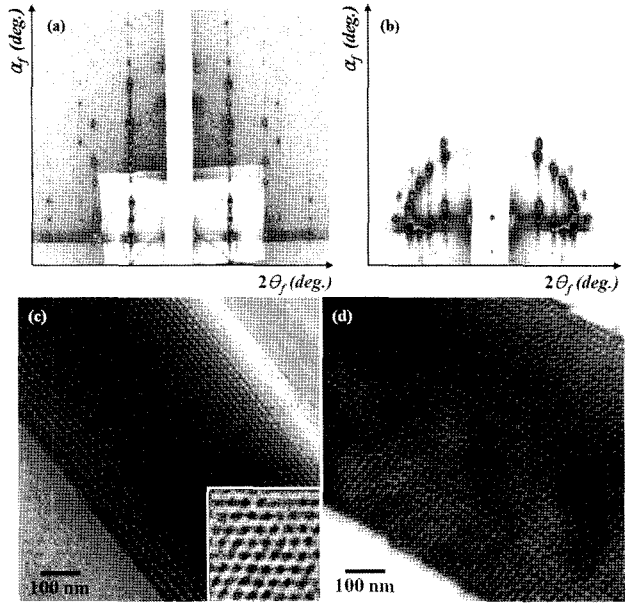

Figure 11. GISAXS patterns of (a) HPL and (b) DG structures. The GISAXS patterns indicate that the layers of HPL and planes of $\{121\}_{DG}$ are parallel to the substrate plane but randomly oriented in-plane. The X-ray beam impinges on the film at an incident angle of 0.22°. Cross-sectional TEM image of (c) HPL and (d) DG structures. The inset in Figure 11(c) is a plan-view TEM image (200 nm×200 nm) of a thinner film (~350 nm thick). Reproduced with permission from Ref. 67; Copyright 2007, ACS publications.

The inset of Figure 11(c) shows a plan-view of a thinner film (~350 nm thick) prepared from a more dilute (5 wt% in toluene) solution. Well-ordered and hexagonally perforated structure is observed. After annealed at higher temperature, the morphology was fully converted to a well-aligned network structure of DG phase as shown in Figure 11(b) and (d).

Although the layer structure and the orientation of the HPL phase are confirmed, the internal structure of the film is not clearly seen from the two-dimensional TEM image. For the three-dimensional imaging of such a structure, TEMT is a powerful tool. Figure 12(a) shows a part of a 3D image of the HPL structure obtained from TEMT.[67] For visual clarity, only the PS domain is shown. The perforations in the layer structure are unambiguously observed. The positional repeating frequency is found in the image: the perforation at the edge of the 1st layer (shown by a vertical arrow) reappears at the same position in the 4th layer. This result indicates that the position of the perforations is repeated every three layers corresponding to the ABC type stacking of the perforations. To make this clearer, three digitally-sliced x-z planes corresponding to the 1st, 3rd and 4th layers are displayed in Figure 12(b). As indicated by the dotted lines in the 1st layer, hexagonally arranged perforations in each layer were apparent. The relative positions of perforations in the three layers were examined in Figure 12(c). The

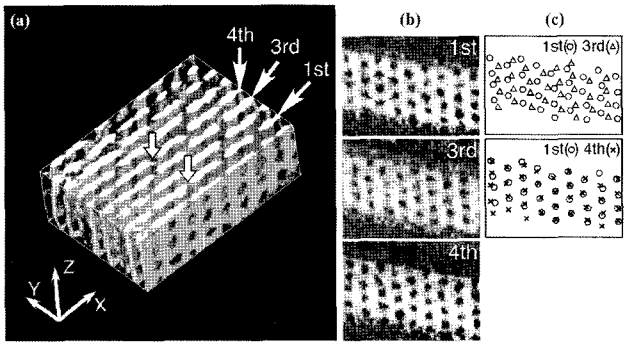

Figure 12. (a) 3D image of the HPL structure obtained by TEMT (260 nm×180 nm×90 nm). Only the PS domain is shown for visual clarity. The vertical arrows indicate the position of the perforations. (b) Digitally-sliced *x-z* planes corresponding to the 1st, 3rd and 4th layers showing the position of the perforations. (c) Overlay of the perforation positions: (Top) 1st and 3rd layers, (Bottom) 1st and 4th layers. The ABC type stacking of the perforation is evident from the matching of the 1st and 4th layers. Reproduced with permission from Ref. 67; Copyright 2007, ACS publications.

1st and 3rd layers exhibit a systematic shift of the perforation positions while the 1st and 4th layers showed a perfect match. Thus, the ABC type stacking, rather than the AB stacking, is evident in the HPL morphology.

The phase transition between DG and HEX structures in block copolymers or in micelles has been studied extensively also.[44,49,53-55,62,66,109,110] There is a consensus that the phase transition between HEX and DG has an epitaxial relationship between $\{121\}_{DG}$ and $\{10\}_{HEX}$, and between $<111>_{DG}$ direction and the HEX cylinder axis, respectively. Most of experimental studies dealt with the phase transition from HEX to DG since the HEX phase can be easily oriented and the aligned HEX structure facilitates the investigation of the structural relationship before and after the phase transition.[44,49,54,55,62,109] Recently, Honda *et al.* reported that a different epitaxial relationship can be found under external field, such as shear field by theoretical study.[66]

We also used PS-*b*-PI thin films for the study of epitaxial relation between DG and HEX.[29] Figure 13 shows the TEM images and GISAXS patterns of DG (a and d), HEX (c and f) and their coexisting phases (b and e) of ~700 nm thick SI film on silicon wafer. TEM images evidence that the block domains in the thin films are well orientated parallel to the substrate plane due to the preferential wetting of PI block. The plane of DG structures shown in Figure 13(a) and (b) are $\{111\}_{DG}$, characterized by the wagon wheel-shaped structure, and that of HEX structures in Figure 13(b) and (c) are $\{11\}_{HEX}$ and the plane perpendicular to the cylinder axis, respectively. According to the TEM images, $\{111\}_{DG}$ and $\{121\}_{DG}$ appears to convert to $\{11\}_{HEX}$ and $\{10\}_{HEX}$, respectively.

The orientation persists in the coexisting structure as can be seen in Figure 13(b) and (e). The diffraction angle of $\{121\}_{DG}$ is very close to that of $\{10\}_{HEX}$. The corresponding interplanar spacing of $\{121\}_{DG}$ and $\{10\}_{HEX}$ are 24.1 nm and 23.8 nm, respectively. However, there is a limit in figuring out the structural relation between DG and HEX from the TEM and GISAXS data because the film has a polycrystalline structure of which in-plane orientation of the grains is random.[12]

Figure 14 shows a 3D-image and its cross sectional images

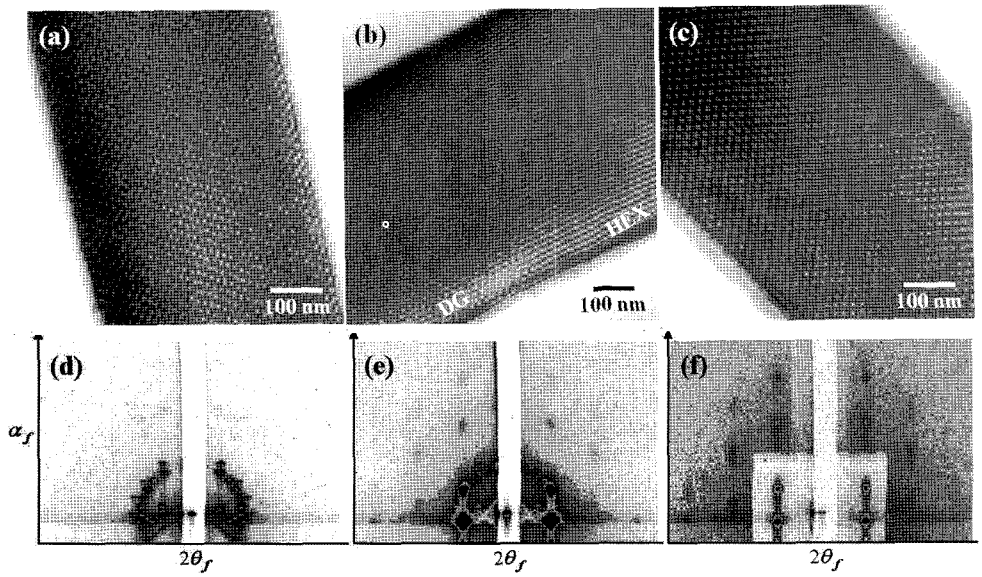

Figure 13. Cross-sectional TEM images and GISAXS patterns of DG (a and d), coexisting structure of DG and HEX (b and e), and HEX (c and f), respectively. GISAXS patterns were acquired at an incident angle of 0.20°. The planes of $\{121\}_{DG}$ and $\{10\}_{HEX}$ are parallel to the substrate and they are epitaxially transformed during the phase transition. Reproduced with permission from the supporting information of Ref. 29; Copyright 2009, ACS publications.

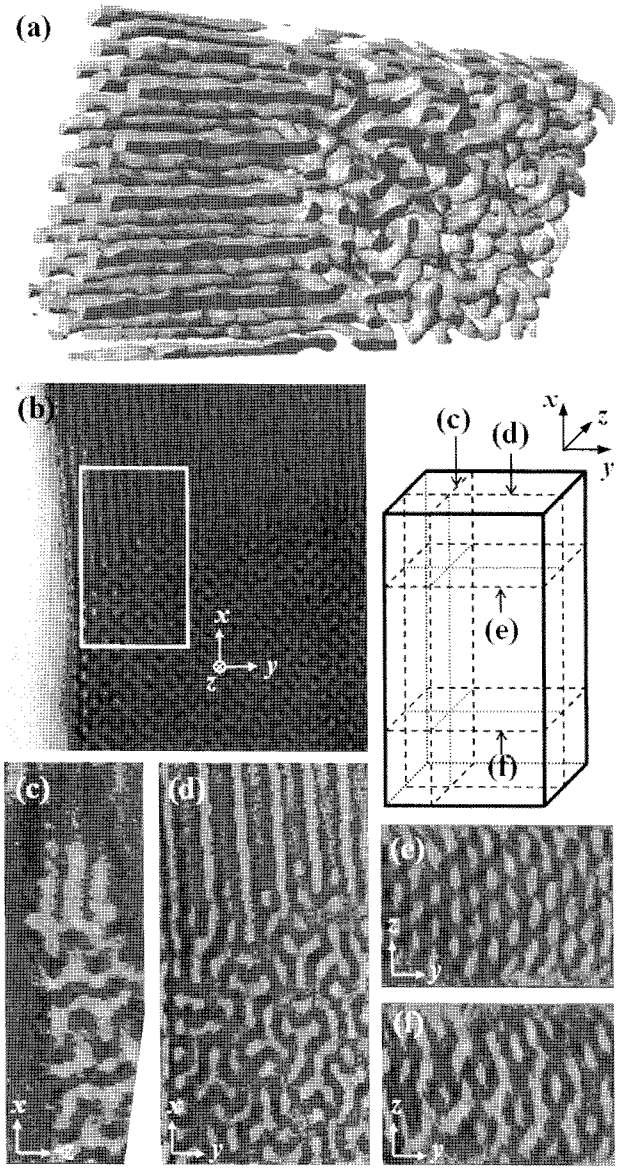

Figure 14. (a) 3D reconstructed image of coexisting structure of DG and HEX. The dimension of the hexahedron is 400, 200, and 80 nm (x, y, z). In this image, only PS domain is shown. (b) TEM image of the sample region from which the 3D image was reconstructed (boxed area). Here, z is the direction of incident electron beam and xz is the film plane. (c)~(f) Images of the cross section illustrated in the hexahedron. PI block was stained with OsO_4 and appears darker. Reproduced with permission from the Ref. 29; Copyright 2009, ACS publications.

of the transitional structure after computerized tomography reconstruction. In the 3D-reconstructed image, Figure 14(a), only PS domain is shown and this hexahedral image was taken from the rectangular box area in the TEM image shown in Figure 14(b). The dimension of the hexahedron is 400 nm, 200 nm, and 80 nm (x, y, z). Here, z is the direction of incident electron beam and xz is the film plane (i.e., substrate surface plane). Figure 14(b) clearly shows the grain boundary region of the coexisting DG and HEX phases. HEX cylinders are oriented nearly along the x axis direction while DG phase shows the $\{111\}_{DG}$ plane characterized by the wagon wheel-like structure.

To better appreciate the 3D-structure of the epitaxial relationship between DG and HEX, several cross-sectional images of the hexahedron are displayed in Figure 14(c-f). The cross sections are illustrated at right of Figure 14(b). Figure 14(e) is a view of the HEX grain perpendicular to the cylinder axis while Figure 14(f) is the image of $\{220\}_{DG}$, which is orthogonal to both $\{121\}_{DG}$ and $\{111\}_{DG}$. It indicates that the HEX cylinder axis is perpendicular to $\{220\}_{DG}$ and parallel to both $\{121\}_{DG}$ and $\{111\}_{DG}$. Figure 14(c) and (d) show the images consistent with this picture. Figure 14(c) shows the coexisting $\{10\}_{HEX}$ and $\{121\}_{DG}$. Figure 14(d) is an expanded version of Figure 14(b), but more clearly shows coexisting $\{11\}_{HEX}$ and $\{111\}_{DG}$ by virtue of being a cross sectional image. Therefore, it is unambiguously confirmed that $\{121\}_{DG}$ and $\{111\}_{DG}$ were converted to $\{10\}_{HEX}$ and $\{11\}_{HEX}$, respectively, which has not been reported in the earlier works.

Summary

Some of the useful tools in the investigation of block copolymers were described in this feature article, which has been utilized in our recent research. Fractionation by 2D-LC is an efficient method to analyze a block copolymer for its distribution in molecular weight as well as in composition. Furthermore, a small scale fractionation is also possible. The LC fractions of an anionic-polymerized diblock copolymer showed a variation of ~15% in average molecular weight as well as ~10% in composition. They make a good set of block copolymers, which have very narrow distribution in both molecular weight and composition within the variation in the average value of 10-20%. For the analysis of transitional structures, TEMT made it possible to observe 3-D inner structure in block copolymer. And it provided local but detailed information on the near-grain boundary structure.

Acknowledgments. This study was supported by KOSEF via NRL (R0A-2007-000-20125-0), SRC (R11-2008-052-03002) and WCU (R31-2008-000-10059-0) programs. The GISAXS measurements at PAL were supported by the Ministry of Science and Technology and POSCO.

References

(1) M. Park, C. Harrison, P. M. Chaikin, R. A. Register, and D. H. Adamson, *Science*, **276**, 1401 (1997).
(2) I. W. Hamley, *The Physics of Block Copolymers*, Oxford Univ. Press, New York, 1998.
(3) T. Thurn-Albrecht, J. Schotter, C. A. Kastle, N. Emley, T.

Shibauchi, L. Krusin-Elbaum, K. Guarini, C. T. Black, M. T. Tuominen, and T. P. Russell, *Science*, **290**, 2126 (2000).
(4) A. Urbas, R. Sharp, Y. Fink, E. L. Thomas, M. Xenidou, and L. J. Fetters, *Adv. Mater.*, **12**, 812 (2000).
(5) C. T. Black, K. W. Guarini, K. R. Milkove, S. M. Baker, T. P. Russell, and M. T. Tuominen, *Appl. Phys. Lett.*, **79**, 409 (2001).
(6) J. Y. Cheng, C. A. Ross, V. Z. H. Chan, E. L. Thomas, R. G. H. Lammertink, and G. J. Vancso, *Adv. Mater.*, **13**, 1174 (2001).
(7) H. C. Kim, X. Q. Jia, C. M. Stafford, D. H. Kim, T. J. McCarthy, M. Tuominen, C. J. Hawker, and T. P. Russell, *Adv. Mater.*, **13**, 795 (2001).
(8) W. Lee, D. Y. Cho, T. Y. Chang, K. J. Hanley, and T. P. Lodge, *Macromolecules*, **34**, 2353 (2001).
(9) S. Park, D. Cho, K. Im, T. Chang, D. Uhrig, and J. W. Mays, *Macromolecules*, **36**, 5834 (2003).
(10) S. Park, I. Park, T. Chang, and C. Y. Ryu, *J. Am. Chem. Soc.*, **126**, 8906 (2004).
(11) B. H. Chung, S. Park, and T. Y. Chang, *Macromolecules*, **38**, 6122 (2005).
(12) B. Lee, I. Park, J. Yoon, S. Park, J. Kim, K. W. Kim, T. Chang, and M. Ree, *Macromolecules*, **38**, 4311 (2005).
(13) I. Park, B. Lee, J. Ryu, K. Im, J. Yoon, M. Ree, and T. Chang, *Macromolecules*, **38**, 10532 (2005).
(14) C. Y. Choi, M. K. Jang, and J. W. Nah, *Macromol. Res.*, **15**, 623 (2007).
(15) K. Dayananda, M. S. Kim, B. S. Kim, and D. S. Lee, *Macromol. Res.*, **15**, 385 (2007).
(16) S. J. Hwang, M. S. Kim, J. K. Han, D. S. Lee, B. S. Kim, E. K. Choi, H. J. Park, and A. S. Kim, *Macromol. Res.*, **15**, 437 (2007).
(17) K. Im, H.-W. Park, Y. Kim, B. Chung, M. Ree, and T. Chang, *Anal. Chem.*, **79**, 1067 (2007).
(18) G. P. Kim, Y. S. Jung, S. B. Yoon, D. W. Kim, and S. H. Baeck, *Macromol. Res.*, **15**, 693 (2007).
(19) S. Y. Kim, S. H. Cho, Y. M. Lee, and L. Y. Chu, *Macromol. Res.*, **15**, 646 (2007).
(20) H. S. Lee, A. Roy, A. S. Badami, and J. E. McGrath, *Macromol. Res.*, **15**, 160 (2007).
(21) Y. K. Lee, S. M. Hong, J. S. Kim, J. H. Im, H. S. Min, E. Subramanyam, and K. M. Huh, *Macromol. Res.*, **15**, 330 (2007).
(22) Y. J. Jun, K. M. Park, Y. K. Joung, K. D. Park, and S. J. Lee, *Macromol. Res.*, **16**, 704 (2008).
(23) B. J. Kim, D. K. Oh, and A. Y. Chang, *Macromol. Res.*, **16**, 103 (2008).
(24) J. K. Kim, J. I. Lee, and D. H. Lee, *Macromol. Res.*, **16**, 267 (2008).
(25) D. H. Lee, Y. S. Kang, J. H. Kim, and S. W. Kang, *Macromol. Res.*, **16**, 676 (2008).
(26) D. K. Lee, J. T. Park, J. K. Choi, D. K. Roh, J. H. Lee, Y. G. Shul, and J. H. Kim, *Macromol. Res.*, **16**, 549 (2008).
(27) Y. Min, S. Lee, J. K. Park, K. Y. Cho, and S. J. Sung, *Macromol. Res.*, **16**, 231 (2008).
(28) S. Park, D. Y. Ryu, J. K. Kim, M. Ree, and T. Chang, *Polymer*, **49**, 2170 (2008).
(29) H.-W. Park, J. Jung, T. Chang, K. Matsunaga, and H. Jinnai, *J. Am. Chem. Soc.*, **131**, 46 (2009).
(30) F. S. Bates, *Science*, **251**, 898 (1991).
(31) F. S. Bates, M. F. Schulz, A. K. Khandpur, S. Foerster, J. H. Rosedale, K. Almdal, and K. Mortensen, *Faraday Discuss.*, **98**, 7 (1994).
(32) C. X. Li, G. H. Li, H. C. Moon, D. H. Lee, J. K. Kim, and J. H. Cho, *Macromol. Res.*, **15**, 656 (2007).
(33) C. Park, M. Rhue, M. Im, and C. Kim, *Macromol. Res.*, **15**, 688 (2007).
(34) C. Park, M. Rhue, J. Lim, and C. Kim, *Macromol. Res.*, **15**, 39 (2007).
(35) J. Bang and T. P. Lodge, *Macromol. Res.*, **16**, 51 (2008).
(36) D. H. Kim, Y. S. Ko, and Y. K. Kwon, *Macromol. Res.*, **16**, 62 (2008).
(37) S. Forster and M. Antonietti, *Adv. Mater.*, **10**, 195 (1998).
(38) A. K. Khandpur, S. Foerster, F. S. Bates, I. W. Hamley, A. J. Ryan, W. Bras, K. Almdal, and K. Mortensen, *Macromolecules*, **28**, 8796 (1995).
(39) L. Leibler, *Marcromolecules*, **13**, 1602 (1980).
(40) M. W. Matsen and F. S. Bates, *Macromolecules*, **29**, 1091 (1996).
(41) K. Almdal, J. H. Rosedale, F. S. Bates, G. D. Wignall, and G. H. Fredrickson, *Phys. Rev. Lett.*, **65**, 1112 (1990).
(42) K. A. Koppi, M. Tirrell, and F. S. Bates, *Phys. Rev. Lett.*, **70**, 1449 (1993).
(43) I. W. Hamley, K. A. Koppi, J. H. Rosedale, F. S. Bates, K. Almdal, and K. Mortensen, *Macromolecules*, **26**, 5959 (1993).
(44) S. Foerster, A. K. Khandpur, J. Zhao, F. S. Bates, I. W. Hamley, A. J. Ryan, and W. Bras, *Macromolecules*, **27**, 6922 (1994).
(45) D. A. Hajduk, P. E. Harper, S. M. Gruner, C. C. Honeker, G. Kim, E. L. Thomas, and L. J. Fetters, *Macromolecules*, **27**, 4063 (1994).
(46) S. Sakurai, H. Kawada, T. Hashimoto, and L. J. Fetters, *Macromolecules*, **26**, 5796 (1993).
(47) D. A. Hajduk, S. M. Gruner, P. Rangarajan, R. A. Register, L. J. Fetters, C. Honeker, R. J. Albalak, and E. L. Thomas, *Macromolecules*, **27**, 490 (1994).
(48) K. A. Koppi, M. Tirrell, F. S. Bates, K. Almdal, and K. Mortensen, *J. Rheol.*, **38**, 999 (1994).
(49) M. F. Schulz, F. S. Bates, K. Almdal, and K. Mortensen, *Phys. Rev. Lett.*, **73**, 86 (1994).
(50) J. Zhao, B. Majumdar, M. F. Schulz, F. S. Bates, K. Almdal, K. Mortensen, D. A. Hajduk, and S. M. Gruner, *Macromolecules*, **29**, 1204 (1996).
(51) M. Laradji, A. C. Shi, J. Noolandi, and R. C. Desai, *Macromolecules*, **30**, 3242 (1997).
(52) N. Sakamoto, T. Hashimoto, C. D. Han, D. Kim, and N. Y. Vaidya, *Macromolecules*, **30**, 1621 (1997).
(53) M. W. Matsen, *Phys. Rev. Lett.*, **80**, 4470 (1998).
(54) M. E. Vigild, K. Almdal, K. Mortensen, I. W. Hamley, J. P. A. Fairclough, and A. J. Ryan, *Macromolecules*, **31**, 5702 (1998).
(55) G. Floudas, R. Ulrich, and U. Wiesner, *J. Chem. Phys.*, **110**, 652 (1999).
(56) I. W. Hamley, J. P. A. Fairclough, A. J. Ryan, S. M. Mai, and C. Booth, *Phys. Chem. Chem. Phys.*, **1**, 2097 (1999).
(57) C. Y. Ryu and T. P. Lodge, *Macromolecules*, **32**, 7190 (1999).
(58) K. Kimishima, T. Koga, and T. Hashimoto, *Macromolecules*, **33**, 968 (2000).
(59) R. Krishnamoorti, A. S. Silva, M. A. Modi, and B. Hammouda, *Macromolecules*, **33**, 3803 (2000).

(60) M. W. Matsen, *J. Chem. Phys.*, **114**, 8165 (2001).
(61) H. H. Lee, W. Y. Jeong, J. K. Kim, K. J. Ihn, J. A. Kornfield, Z. G. Wang, and S. Y. Qi, *Macromolecules*, **35**, 785 (2002).
(62) C. Y. Wang and T. P. Lodge, *Macromolecules*, **35**, 6997 (2002).
(63) J. H. Ahn and W. C. Zin, *Macromol. Res.*, **11**, 152 (2003).
(64) S. Park, K. Kwon, D. Cho, B. Lee, M. Ree, and T. Chang, *Macromolecules*, **36**, 4662 (2003).
(65) L. Zhu, P. Huang, W. Y. Chen, X. Weng, S. Z. D. Cheng, Q. Ge, R. P. Quirk, T. Senador, M. T. Shaw, E. L. Thomas, B. Lotz, B. S. Hsiao, F. J. Yeh, and L. Z. Liu, *Macromolecules*, **36**, 3180 (2003).
(66) T. Honda and T. Kawakatsu, *Macromolecules*, **39**, 2340 (2006).
(67) H.-W. Park, K. Im, B. Chung, M. Ree, T. Chang, K. Sawa, and H. Jinnai, *Macromolecules*, **40**, 2603 (2007).
(68) F. S. Bates, K. A. Koppi, M. Tirrell, K. Almdal, and K. Mortensen, *Macromolecules*, **27**, 5934 (1994).
(69) M. Szwarc, *Nature*, **178**, 1168 (1956).
(70) H. L. Hsieh and R. P. Quirk, *Anionic Polymerization: Principles and Practical Applications*, Marcel-Dekker, New York, 1996.
(71) A. Hasneen, S. J. Kim, and H. J. Paik, *Macromol. Res.*, **15**, 541 (2007).
(72) D. H. Go, H. J. Jeon, T. H. Kim, G. Kim, J. H. Choi, J. Y. Lee, and J. Kim, *Macromol. Res.*, **16**, 659 (2008).
(73) K. M. Kim, S. Y. Choi, H. J. Jeon, J. Y. Lee, D. J. Choo, J. Kim, Y. S. Kang, and H. O. Yoo, *Macromol. Res.*, **16**, 169 (2008).
(74) S. D. Park, W. Xu, C. Chung, and Y. Kwon, *Macromol. Res.*, **16**, 155 (2008).
(75) J. H. You, S. W. Choi, J. H. Kim, and Y. T. Kwak, *Macromol. Res.*, **16**, 609 (2008).
(76) W. W. Yau, J. J. Kirkland, and D. D. Bly, *Modern Size-Exclusion Liquid Chromatography, Practice of Gel Permeation and Gel Filtration Chromatograph*, John Wiley & Sons, New York, 1979.
(77) S. Mori and H. G. Barth, *Size Exclusion Chromatography*, Springer-Verlag, New York, 1999.
(78) H. Cho, S. Park, M. Ree, T. Chang, J. C. Jung, and W. C. Zin, *Macromol. Res.*, **14**, 383 (2006).
(79) H. C. Lee and T. Chang, *Polymer*, **37**, 5747 (1996).
(80) H. C. Lee, W. Lee, and T. Chang, *Korea Polym. J.*, **4**, 160 (1996).
(81) T. Chang, H. C. Lee, W. Lee, S. Park, and C. Ko, *Macromol. Chem. Phys.*, **200**, 2188 (1999).
(82) T. Chang, *Adv. Polym. Sci.*, **163**, 1 (2003).
(83) T. Chang, *J. Polym. Sci. Part B: Polym. Phys.*, **43**, 1591 (2005).
(84) J. Ryu and T. Chang, *Anal. Chem.*, **77**, 6347 (2005).
(85) W. Lee, H. Lee, J. Cha, T. Chang, K. J. Hanley, and T. P. Lodge, *Macromolecules*, **33**, 5111 (2000).
(86) P. J. Flory, *J. Am. Chem. Soc.*, **62**, 1561 (1940).
(87) H. Jinnai, Y. Nishikawa, T. Ikehara, and T. Nishi, *NMR - 3D Analysis - Photopolymerization*, **170**, 115 (2004).
(88) H. Dohi, H. Kimura, M. Kotani, T. Kaneko, T. Kitaoka, T. Nishi, and H. Jinnai, *Polym. J.*, **39**, 749 (2007).
(89) V. H. Mareau, S. Akasaka, T. Osaka, and H. Hasegawa, *Macromolecules*, **40**, 9032 (2007).
(90) K. Im, H. W. Park, Y. Kim, and T. Chang, *Macromol. Res.*, **16**, 544 (2008).
(91) H. C. Lee and T. H. Chang, *Macromolecules*, **29**, 7294 (1996).
(92) W. Lee, D. Cho, B. O. Chun, T. Chang, and M. Ree, *J. Chromatogr. A*, **910**, 51 (2001).
(93) S. Park, D. Cho, J. Ryu, K. Kwon, W. Lee, and T. Chang, *Macromolecules*, **35**, 5974 (2002).
(94) G. Glockner, *Gradient HPLC of Copolymers and Chromatographic Cross-Fractionation*, Springer -Verlag, Berlin, 1992.
(95) H. Pasch and B. Trathnigg, *HPLC of Polymers*, Springer-Verlag, Berlin, 1997.
(96) D. Berek, *Prog. Polym. Sci.*, **25**, 873 (2000).
(97) K. Im, H.-W. Park, S. Lee, and T. Chang, *J. Chromatogr. A*, **1216**, 4606 (2009).
(98) J.-H. Ahn and W.-C. Zin, *Macromolecules*, **33**, 641 (2000).
(99) J. H. Rosedale and F. S. Bates, *Macromolecules*, **23**, 2329 (1990).
(100) K. Almdal, K. A. Koppi, F. S. Bates, and K. Mortensen, *Macromolecules*, **25**, 1743 (1992).
(101) N. P. Balsara, D. Perahia, C. R. Safinya, M. Tirrell, and T. P. Lodge, *Macromolecules*, **25**, 3896 (1992).
(102) J. K. Kim, H. H. Lee, and K. B. Lee, *Polym. Mater. Sci. Eng.*, **79**, 330 (1998).
(103) S.-H. Lee and K. Char, *Polym. Mater. Sci. Eng.*, **79**, 314 (1998).
(104) T. P. Lodge, B. Pudil, and K. J. Hanley, *Macromolecules*, **35**, 4707 (2002).
(105) H. Kiessig, *Ann. Phys.*, **10**, 769 (1931).
(106) L. G. Parratt, *Phys. Rev.*, **95**, 359 (1954).
(107) T. P. Russell, *Mater. Sci. Rep.*, **5**, 171 (1990).
(108) J. Yoon, K. W. Kim, J. Kim, K. Heo, K. S. Jin, S. Jin, T. J. Shin, B. Lee, Y. Rho, B. Ahn, and M. Ree, *Macromol. Res.*, **16**, 575 (2008).
(109) Y. Rancon and J. Charvolin, *J. Phys. Chem.*, **92**, 2646 (1988).
(110) M. Clerc, A. M. Levelut, and J. F. Sadoc, *J. Phys. II*, **1**, 1263 (1991).